Structures induced by small moonlets in Saturn's rings: Implications for the Cassini Mission

M. Seiß,[1] F. Spahn,[1] M. Sremčević,[1,3] and H. Salo[2]

Received 21 January 2005; revised 22 April 2005; accepted 5 May 2005; published 15 June 2005.

[1] Particle simulations are carried out to study density features caused by small moonlets embedded in a dense planetary ring. The creation of a "propeller" like structure is found together with adjacent density wakes. Both features are clear indications for the existence of moonlets in the rings. We confirmed that the propeller scales with the Hill-radius in radial direction whereas its azimuthal extent is determined by the ratio between the moonlet-mass and the ring-viscosity. Our findings bear direct implications for the analysis of the Cassini imaging (ISS) and occultation (UVIS) data: (i) for the detection of embedded larger bodies (>30 m) in Saturn's rings, and (ii) for remotely probing transport properties of the rings. The existence of a moonlet population may point to a catastrophic disruption of a parent body as a formation scenario for rings. **Citation:** Seiß, M., F. Spahn, M. Sremčević, and H. Salo (2005), Structures induced by small moonlets in Saturn's rings: Implications for the Cassini Mission, *Geophys. Res. Lett.*, *32*, L11205, doi:10.1029/2005GL022506.

1. Introduction

[2] Saturn's dense rings consist of icy particles ranging in size from a few centimeters up to several meters. Furthermore, some bigger bodies are also expected to exist in the rings with sizes of tens of meters up to kilometers. It is known that the gravity of moonlets produce density wakes [*Cuzzi and Scargle*, 1985; *Showalter et al.*, 1986; *Lewis and Stewart*, 2000], gaps with a ringlet covering the moonlet orbit [*Henon*, 1981; *Lissauer et al.*, 1981; *Spahn and Wiebicke*, 1989; *Hänninen*, 1993] and S-shaped density structures (propellers) [*Spahn and Sremčević*, 2000; *Sremčević et al.*, 2002]. Theories about gaps and wakes combined with the analysis of Voyager data predicted a few satellites in Saturn's rings [*Lissauer et al.*, 1981; *Showalter et al.*, 1986; *Spahn and Sponholz*, 1989]. However, only a single satellite (Pan) has been finally found in the Encke division [*Showalter*, 1991].

[3] A probabilistic scattering model [*Spahn and Wiebicke*, 1989] predicted a formation of a gap in the region $|b| \leq 4$ divided by a narrow ringlet covering the orbit of the moon at $|b| = 0$. The impact parameter $b = (r - a_0)/h = x/h$ and the radial features can be scaled by the Hill radius

$$h = \frac{a_0}{R_s}\left(\frac{\rho_m}{3\rho_s}\right)^{1/3} \cdot R_m. \tag{1}$$

The densities and radii of moonlet and Saturn as well as the semi-major axis are denoted by ρ_m, ρ_s, R_m, R_s and a_0, respectively.

[4] However, the model of *Spahn and Wiebicke* [1989] is inappropriate for smaller moonlets. In this case viscous diffusion of particles becomes important, counteracting the tendency of the moonlet to create a gap. Therefore, *Spahn and Sremčević* [2000] and *Sremčević et al.* [2002] (hereinafter referred to as SpSr and SSD) extended the theory of gravitational scattering to diffusion of the ring material in the radial direction, described by mass- and momentum balances. Solutions of the related nonlinear diffusion equation revealed a scaling of the azimuthal direction as

$$K = \frac{\Omega_0 h^3}{2(1+\beta)\nu_0 a_0}, \tag{2}$$

giving the scaled azimuthal coordinate $\phi = y/(a_0 K)$, whereas y is the azimuthal distance from the moonlet. The Keplerian frequency is defined by $\Omega_0 = \sqrt{GM_s/a_0^3}$. The scaling parameter K is determined by the ratio $h^3/\nu_0 \propto M_m/\nu_0$, where ν_0 denotes the kinematic viscosity. Knowing the moonlet mass M_m from the radial features of the S-shaped propeller structure, an analysis of the azimuthal structures enables to estimate the viscosity ν_0. The coefficient $\beta \approx 1$ arises from the viscosity model $\nu = \nu_0 \cdot (\tau/\tau_0)^\beta$ [*Schmit and Tscharnuter*, 1995; *Salo et al.*, 2001], where τ is the optical depth of the ring. In spite of the improvement of the scattering model due to the consideration of dissipative processes, some restrictive assumptions have been necessary for its derivation. For instance, (i) the scattering region is reduced to a line, (ii) the collisions are neglected during the scattering and (iii) the azimuthal velocity component is taken to be the Keplerian circular velocity beyond the scattering line. Thus, the model of gravitational scattering does not account for moonlet density-wakes.

[5] In order to check the influence of these simplifications, to verify previous predictions (SSD) and to extend them to small moonlet sizes, we carry out N-body simulations. This alternative approach allows to investigate the influence of the moonlet induced wakes on the propeller as well as to resolve the density structures inside the scattering region.

2. Method

[6] For the N-body simulations we use the local method, first introduced for rings by *Wisdom and Tremaine* [1988]

[1]Department of Physics, Nonlinear Dynamics, University of Potsdam, Potsdam, Germany.
[2]Department of Physical Science, Astronomy Division, University of Oulu, Oulu, Finland.
[3]Now at Laboratory for Atmospheric and Space Physics, University of Colorado, Boulder, Colorado, USA.

Copyright 2005 by the American Geophysical Union.
0094-8276/05/2005GL022506$05.00

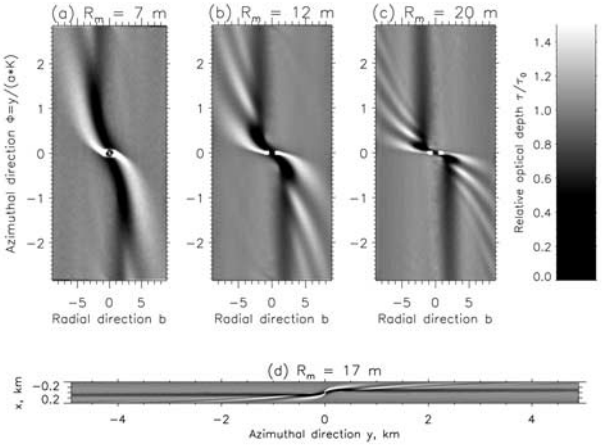

Figure 1. Steady-state density response for different sized moonlets. The plots are shown in scaled coordinates (a) R_m = 7 m, (b) R_m = 12 m and (c) R_m = 20 m. Part (d) shows the resulting density of a R_m = 17 m moonlet in physical units with a correct aspect ratio, i.e. how it might appear in Cassini imaging data.

and further elaborated by *Salo* [1991, 1995]. The box, with half-widths L_x and L_y in radial and azimuthal directions, is filled with N particles, representing a dynamical optical depth $\tau = \pi N R^2/(4L_xL_y)$. Tests suggest $L_x = 9h$ and $L_y = 2.8\ Ka_0$ to be the optimum size of the calculation box - large enough to cover the main structures and still manageable numerically. We fixed τ to 0.08, requiring N = 2,900–190,000 particles for moonlet radii R_m = 7–20 m. The choice of R_m and τ is solely limited by the computer performance. However the scalings work even better for larger moonlets. The value τ = 0.08 fits conditions of the C-ring, nevertheless the results can be applied to denser regions (A and B ring) using the scaling laws for the adapted viscosity.

[7] The particles are modeled by inelastic hard spheres with radius R = 1 m. A semi-major axis of $a_0 = 10^8$ m has been used, corresponding to $h = 1.35\ R_m$ for an icy moonlet (ρ_m = 900 kg m^{-3}). However, the results can be scaled to other planetocentric distances provided that $h/R_m \propto a_0\rho_m^{1/3}$ is fixed. A constant coefficient of restitution $\epsilon = 0.5$ has been chosen for the collisions. Apart from the inelastic collisions, the motion of the particles around the moonlet is described by the Hill equations [e.g., *Salo*, 1991]. The moonlet is placed in the center of the box. The gravity between the particles is not taken into account. The effect of self-gravity is approximated via an enhanced vertical frequency $\Omega_z = 3.6\Omega_0$ [*Wisdom and Tremaine*, 1988; *Salo*, 1991]. Thus, the simulations can not account for the spontaneous creation of gravitational wakes produced by the gravity of the small ring particles [*Salo*, 1992, 1995]. Self-gravity effects are discussed in section 4.

[8] Usually periodic boundary conditions are used in the radial as well as in the azimuthal direction [*Wisdom and Tremaine*, 1988; *Salo*, 1991, 1995]. Because we are not able to simulate the whole azimuthal extent of the propeller, the particles are still perturbed by the moonlet when they leave the calculation region. Therefore the incoming flux of particles would not correspond to an unperturbed ring flow. To avoid this, we drop the azimuthal periodic boundary conditions and utilize separate simulations without a moonlet, but with periodic boundary conditions to sample the unperturbed velocity distribution. Then, we use this data (particles' position and velocity while crossing the boundary) to simulate the incoming flow of the perturbed simulation cell at the azimuthal boundaries. In the radial direction we retain the periodic boundary condition.

3. Results

[9] Figures 1a–1c show the optical depth τ for simulations with different moonlets (R_m = 7, 12, 20 m). All figures show a S-shaped propeller structure. The moonlet tries to generate a gap whereas collisional diffusion replenishes the material along increasing azimuth $\phi = y/(a_0K)$. Density wakes evolve adjacent to the propeller ($|b| \geq 2$). The phase of the wakes does not scale with K, but rather with azimuthal wave number $|\tilde{m}| = 2a_0/(3hb)$ [*Showalter et al.*, 1986].

[10] Figure 1d shows the propeller of a R_m = 17 m sized moonlet as it might be seen with high resolution cameras. The extension of the propeller is much larger in the azimuthal direction than in the radial one. The moonlet location is indicated by the kink in the gap at $\phi = b = 0$.

[11] To check the scalings of the structure, in Figure 2 the radial and azimuthal profiles corresponding to different R_m have been plotted using scaled units. All radial profiles have been averaged over the azimuth in order to cancel wake effects. Furthermore we excluded the region where the

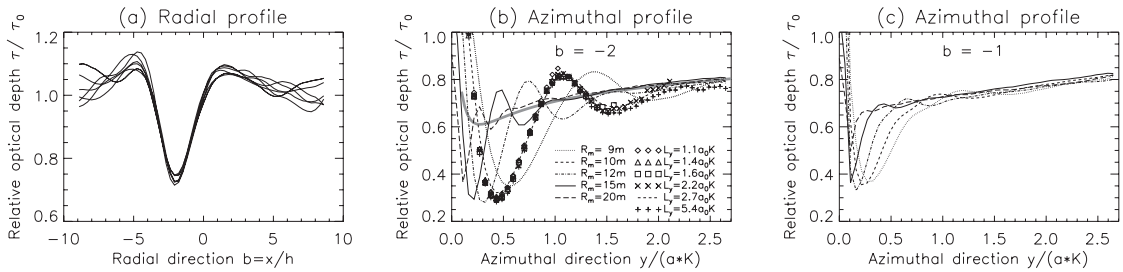

Figure 2. Radial and azimuthal profiles of the propeller. Part (a) shows the azimuthally averaged radial profile (for $\phi > 1$) for moonlet radii R_m = 9–20 m. Part (b) shows the azimuthal profile at b = −2 scaled by $a_0 \cdot K$. Only the quadrant of the perturbed outgoing particles is presented ($b < 0$ and $\phi > 0$). The thick gray solid line represents the approximate analytical solution (Figure 10c of SSD). The other lines are simulation data for different sized moonlets and the symbols correspond to simulations of a R_m = 10 m moonlet, but with different azimuthal box size. The plot (c) illustrates the azimuthal profile at $b = -1$.

moonlet gravity dominates the structure ($\phi < 1$). Figure 2a shows a good agreement between the radial profiles for all different moonlets. The minimum of the gap is located at $|b| = 2$, like in the simulations without diffusion [*Spahn and Wiebicke*, 1989].

[12] Figure 2b shows the azimuthal profiles for a cut at the minimum of the gap at $|b| = 2$. Beyond a critical value $\phi > \phi_c(M_m)$, denoting the region of gravitational influence of the moonlet, all profiles converge to almost a single line. A good agreement is found with the theoretical prediction by SpSr and SSD indicating that the azimuthal extent scales with K. We also fitted the analytical solution (see Figure 10c of SSD) in the numerical results (gray line), which provides an estimate of the azimuthal scale $K = 0.14\ \mathrm{m}^{-2} \cdot h^3/a_0$. This value K corresponds to a viscosity $\nu_{0,p} = 3\ \mathrm{cm}^2\ \mathrm{s}^{-1}$ in the perturbed region, assuming $\beta \approx 1$. We measured a viscosity of $\nu_{0,u} = 1.2\ \mathrm{cm}^2\ \mathrm{s}^{-1}$ in the unperturbed cell. Both measured viscosities are of the same order of magnitude, suggesting a fair agreement between simulations and theory. The difference in both values ν_0 are caused by the simplifying assumptions made in the analytical model. The perturbed optical depth varies between $\tau/\tau_0 = 0.2-1.3$ violating the assumption of small deviations made in SSD. For such considerable variations the coefficient β is no more constant [*Salo et al.*, 2001].

[13] The symbols in the Figure 2b represent simulations with $R_m = 10$ m, but using different azimuthal box sizes ($L_y = 1-5.4\ Ka_0$). The results agree quite well, demonstrating the independence of our results with respect to the box size. Figure 2c represents a cut at $|b| = 1$. At this radial position the density depletion is still noticeable, but the wakes do not influence the profile. Here the convergence of the lines for growing azimuthal length is even more impressive.

[14] At smaller azimuthal longitudes the scaling does not work anymore because of the finite size of the scattering region and the stronger dominance of the wakes in the gap. The critical value $\phi_c(M_m) \approx 50 \cdot h/(a_0\ K) \propto h^{-2}$ shrinks with increasing moonlet mass, indicating that the concept of a scattering line mimicking the Hill sphere becomes more realistic for larger moonlets (see also Figures 1a–1c).

[15] Figures 3a–3c show a zoomed part of the region of interest whereas the analytical solution (SSD) is plotted in Figure 3d for comparison. The wakes are still prominent in the region of the gap up to $|b| \geq 2$ in contrast to the wake model [*Showalter et al.*, 1986] where wakes occur at $|b| \geq 4$. Of course, the wakes cannot be described with the scattering model, because azimuthal structures are averaged out, except for the gap. On the other hand, our numerical experiments take into account all those effects leading to a propeller interfered by moonlet wakes – a pattern which can be expected to show up in Saturn's rings provided larger bodies exist there. In all cases, the maximal extent in the azimuthal direction of the contour lines agree well with each other, confirming the scaling predicted by theory. This is even more astonishing having in mind that the azimuthal length of the figures represent 340 m for $R_m = 7$ m in contrast to 8000 m for $R_m = 20$ m.

4. Discussion

[16] Simulations have been run with different sized embedded moons $R_m = 7-20$ m. Larger moonlets, higher optical depths as well as self-gravity could not be included because of the limiting computer performance. On the other hand the analytical model becomes more realistic for larger moonlets. In that view our current results are very encouraging. The scalings seem to be valid for simulated moonlet sizes and are expected to work even better for larger bodies $R_m = 30-500$ m. Further it has been shown that the moonlet induced wakes do not noticeably influence the scaling laws of the propeller. The model (SSD) predicts that the threshold moonlet size separating propeller and gap is $R_m = 500\ \mathrm{m} \cdot [\nu_0/10\ \mathrm{cm}^2\ \mathrm{s}^{-1}]^{1/3}$. Larger moonlets are able to sweep free a complete gap, but the characteristic kink vanishes, and thus, they are probably harder to associate with moonlets.

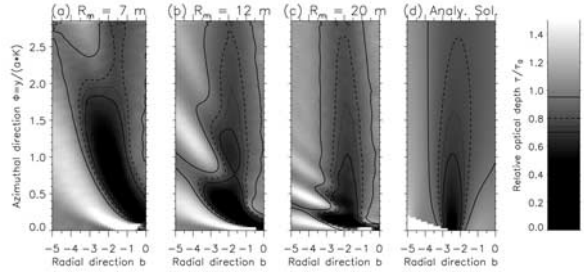

Figure 3. Gray-coded densities with overplotted isolines for different sized moonlets. Panels (a)–(c) show the resulting density fields for R_m = 7 m, 12 m, 20 m, whereas (d) represents the analytical solution (Figure 10c of SSD).

[17] The self-gravity, not considered here, deserves separate attention, because it influences the transports and causes density wakes which might change the picture outlined here. Self gravity wakes are characterized by the critical wavelength $\lambda_{cr} \approx 100$ m and the pitch angle $\alpha = 20°-25°$ [*Salo*, 1995]. The gap width of the propeller is approximately $2.5h$ and becomes larger than λ_{cr} for $R_m = 30$ m. For $R_m > 100$ m the characteristic length scales of the propeller $L_r = 10h \approx 1.3$ km and $L_\phi = 2 \cdot 50\ Ka_0 \approx 4 \cdot 10^4$ km ($\nu_0 = 3\ \mathrm{cm}^2\ \mathrm{s}^{-1}$, $\beta = 1$; compare SSD) exceed by far λ_{cr}. The pitch angle of the gravity-wakes can be compared with the ratio of the propeller extensions $\tan\alpha = L_r/L_\phi \propto h^{-2}$. Boulders with $R_m = 0.5-5$ m ($\nu_0 = 1-100\ \mathrm{cm}^2\ \mathrm{s}^{-1}$, $\beta = 1$) would show tilts comparable to that of gravity wakes. However, we are interested in propellers caused by larger moonlets ($R_m > 30$ m) which are azimuthally elongated structures in contrast to the tilted wakes. Self-gravity wakes are expected to superimpose the propeller-wake structure by overlaying a fine scale pattern. Further the self-gravity modified viscosity [*Daisaka et al.*, 2001] increases the efficiency of the radial transports, thus the maximal moonlet size for propeller formation might in fact be a bit larger than 500 m anticipated above: e.g. $\nu_0 = 100\ \mathrm{cm}^2\ \mathrm{s}^{-1}$ would roughly double the size. Summarizing, we argue that the propellers and wakes created by moonlets $R_m > 30$ m can be slightly modified but likely not destroyed by the self-gravity effects.

[18] On 1 July 2004 Cassini arrived at Saturn and started delivering data with unprecedented resolution. This offers a great chance to discover moonlets (200–500 m) embedded in the rings, by applying the results of our simulations - especially scalings confirmed here - to the ISS imaging and the UVIS occultation data of the Cassini spacecraft, provided that such bodies exist in the rings. In this context characteristic features, especially the kink of the structure

found with our numerical experiments, could reveal the location of the moonlet in the narrow angle images. There the radial location of the gap minimum changes suddenly from about $-2h$ to $+2h$. The absolute scale of this 'jump' corresponds to 1000 m for R_m = 200 m and to 2500 m for R_m = 500 m. For comparison, the published imaging data of Cassini at Saturn orbit insertion (SOI) had their highest spatial resolution of about 200–300 m, so that moonlets of two hundred meter in size mark the limit of the detectability.

[19] What might be the probability to detect a moonlet in a Cassini image? Consider that the particle size distribution could be modeled by a two sided power law $n(R) \propto R^{-q}$, e.g. assuming the ring has been formed by a catastrophic disruption of a parent body. *French and Nicholson* [2000] estimated $q = 2.9$ for particles $R = 1$ cm–20 m from stellar occultation observations of the outer A-ring. A sharp knee is expected in the distribution showing a steeper slope for larger particles $R > 20$ m. Provided that the moonlet Pan is the largest fragment of the disruption a power law with $q \approx 6$ would be plausible for particles $R > 20$ m [*Cuzzi et al.*, 1984], but also $q \approx 7$ or 8 are conceivable. Density structures of moonlets $R_m > 200$ m can be discovered in the high resolution SOI images. The detection probability of this size class can be estimated to 0.1–13 bodies per image for $\tau = 0.5$, assuming the power law holds in this range. Parameters of the inner A and the B ring would roughly double the predicted number of moonlets, promising a good chance to find one, provided such a moonlet population exists. However, it has to be noted that a direct extrapolation of such a distribution to larger sizes would imply more than 100 moonlets with $R_m > 500$ m in the A and B rings, thus being able to clear gaps. This seems to be ruled out by the fact that almost no empty gaps (except Encke and Keeler gaps) are known in these rings. Nevertheless if the largest particles of the continuous distribution are 20m, a small number of larger bodies can not be excluded to exist in the rings.

[20] An alternative method to find signatures of an embedded moonlet is to analyze UVIS occultation data. UVIS data are much higher in resolution (≈20 m [*Esposito et al.*, 1998]; similar to RSS ≈10 m [*Kliore et al.*, 2004]) but only one dimensional. Here the moonlet can be uncovered by the characteristic radial propeller shape (Figure 2a), but it is harder to distinguish them from other structures in the ring. Thus, the best approach would be at first to search for indications in the imaging data and then to analyse UVIS optical depth profiles in detail. Additionally, propeller structures could superpose each other and provide an alternative explanation for the radial fine structure seen in some Cassini images [see *Porco et al.*, 2005, Figures 5a and 5f], beside instabilities [*Schmit and Tscharnuter*, 1995; *Schmidt and Salo*, 2003]. All in all, even if the existence and distribution of moonlets is quite uncertain, it is an interesting challenge to check the ISS and UVIS data on the base of our results.

[21] Once a propeller has been identified in the ISS or UVIS data the analysis of the the propeller shape can deduce the mass of the moonlet as well as the viscosity of the ring material from the scalings laws. Finally, if enough moonlets were found, it would become possible to gain information about the distribution of such bodies, containing hints about the origin of Saturn's rings.

[22] **Note added in proof.** In May 2005 a satellite (S/2005 S1) has been detected inside the Keeler gap, showing the pairwise wakes seen in Figure 1 and confirming the expected radial scaling.

[23] **Acknowledgments.** We thank Jürgen Schmidt for many useful discussions and L. Dones and J. A. Burns for their helpful reviews. This work was supported by the Deutsche Forschungsgemeinschaft (DFG), Deutsches Zentrum für Luft- und Raumfahrt (DLR), Väisälä Foundation and the Academy of Finland.

References

Cuzzi, J. N., and J. D. Scargle (1985), Wavy edges suggest moonlet in Encke's gap, *Appl. Phys. J.*, *292*, 276–290.
Cuzzi, J. N., et al. (1984), Saturn's rings: Properties and processes, in *Planetary Rings*, edited by R. Greenberg and A. Brahic, pp. 73–199, Univ. of Ariz. Press, Tucson.
Daisaka, H., H. Tanaka, and S. Ida (2001), Viscosity in a dense planetary ring with self-gravitating particles, *Icarus*, *154*, 296–312.
Esposito, L. W., J. E. Colwell, and W. E. McClintock (1998), Cassini UVIS observations of Saturns rings, *Planet. Space. Sci.*, *46*, 1221–1235.
French, R. G., and P. D. Nicholson (2000), Saturn's rings II. Particle sizes inferred from stellar occultation data, *Icarus*, *145*, 502–523.
Hänninen, J. (1993), Numerical simulations of moon-ringlet interaction, *Icarus*, *103*, 104–123.
Henon, M. (1981), A simple model of Saturn's rings, *Nature*, *293*, 33–35.
Kliore, A. J., et al. (2004), Cassini radio science, *Space Sci. Rev.*, *115*, 1–4.
Lewis, M. C., and G. R. Stewart (2000), Collisional dynamics of perturbed planetary rings. I, *Astron. J.*, *120*, 3295–3310.
Lissauer, J. J., F. H. Shu, and J. N. Cuzzi (1981), Moonlets in Saturn's rings, *Nature*, *292*, 707–711.
Porco, C. C., et al. (2005), Cassini imaging science: Initial results on Saturn's rings and small satellites, *Science*, *307*, 1226–1236.
Salo, H. (1991), Numerical simulations of dense collisional systems, *Icarus*, *90*, 254–270.
Salo, H. (1992), Gravitational wakes in Saturn's rings, *Nature*, *359*, 619–621.
Salo, H. (1995), Simulations of dense planetary rings, III. Self-gravitating identical particles, *Icarus*, *117*, 287–312.
Salo, H., J. Schmidt, and F. Spahn (2001), Viscous overstability in Saturn's B ring. I. Direct simulations and measurement of transport coefficients, *Icarus*, *153*, 295–315.
Schmidt, J., and H. Salo (2003), Weakly nonlinear model for oscillatory instability in Saturn's dense rings, *Phys. Rev. Lett.*, *90*(6), doi:10.1103/PhyRevLett.90.061102.
Schmit, U., and W. M. Tscharnuter (1995), A fluid dynamical treatment of the common action of self-gravitation, collisions, and rotation in Saturn's B-ring, *Icarus*, *115*, 304–319.
Showalter, M. R. (1991), Visual detection of 1981S13, Saturn's eighteenth satellite, and its role in the Encke gap, *Nature*, *351*, 709–713.
Showalter, M. R., J. N. Cuzzi, E. A. Marouf, and L. W. Esposito (1986), Satellite "wakes" and the orbit of the Encke Gap moonlet, *Icarus*, *66*, 297–323.
Spahn, F., and H. Sponholz (1989), Existence of moonlets in Saturn's rings inferred from the optical depth profile, *Nature*, *339*, 607–608.
Spahn, F., and M. Sremčević (2000), Density patterns induced by small moonlets in Saturn's rings?, *Astron. Astrophys.*, *358*, 368–372.
Spahn, F., and H.-J. Wiebicke (1989), Long-term gravitational influence of moonlets in planetary rings, *Icarus*, *77*, 124–134.
Sremčević, M., F. Spahn, and W. J. Duschl (2002), Density structures in perturbed thin cold discs, *Mon. Not. R. Astron. Soc.*, *337*, 1139–1152.
Wisdom, J., and S. Tremaine (1988), Local simulations of planetary rings, *Astron. J.*, *95*, 925–940.

H. Salo, Department of Physical Science, Astronomy Division, University of Oulu, FIN-90014 Oulun Yliopisto, Finland.
M. Seiß and F. Spahn, Department of Physics, Nonlinear Dynamics, University of Potsdam, Am Neuen Palais 10, Haus 19, D-14469 Potsdam, Germany. (martins@agnld.uni-potsdam.de)
M. Sremčević, LASP, University of Colorado, 1234 Innovation Drive, Boulder, CO 80303, USA.